Moving a Microtubule May Require Two Heads: A Kinetic Investigation of Monomeric Ncd †

ARTICLE *in* BIOCHEMISTRY · MARCH 2000

Impact Factor: 3.02 · DOI: 10.1021/bi991918+ · Source: PubMed

2 AUTHORS:

Andrew Mackey
Mondelēz International
10 PUBLICATIONS **399** CITATIONS
SEE PROFILE

Susan P Gilbert
Rensselaer Polytechnic Institute
80 PUBLICATIONS **2,814** CITATIONS
SEE PROFILE

Moving a Microtubule May Require Two Heads: A Kinetic Investigation of Monomeric Ncd†

Andrew T. Mackey and Susan P. Gilbert*

Department of Biological Sciences, 518 Langley Hall, University of Pittsburgh, Pittsburgh, Pennsylvania 15260

Received August 16, 1999; Revised Manuscript Received November 22, 1999

ABSTRACT: Ncd is a minus-end-directed microtubule motor and a member of the kinesin superfamily. The Ncd dimer contains two motor domains, and cooperative interactions between the heads influence the interactions of each respective motor domain with the microtubule. The approach we have taken to understand the cooperativity between the two motor domains is to analyze the ATPase cycle of dimeric MC1 and monomeric MC6. The steps in the ATPase cycle where cooperativity occurs can be identified by comparing the two mechanisms. The rate-limiting step in the MC6 mechanism is ADP release at 3.4 s^{-1}. The observed rate constant for ATP-induced dissociation from the microtubule is 14 s^{-1}. However, the relative amplitude associated with MC6 dissociation is extremely small in comparison to the amplitude associated with dimeric MC1 dissociation kinetics. The amplitude data indicate that monomeric MC6 does not detach from the microtubule during the initial turnovers of ATP, and ATP hydrolysis is uncoupled from movement. The results show that cooperative interactions between the motor domains of the dimer are required for ATP-dependent dissociation; therefore, one function of the partner motor domain may be to weaken the interaction of the adjacent head with the microtubule.

Nonclaret disjunctional protein (Ncd)[1] is a C-terminal molecular motor in the kinesin superfamily identified in *Drosophila melanogaster* (*1*, *2*). This protein was found to be a key component of the meiotic spindle during oogenesis and the mitotic spindle during the early cleavages of the *Drosophila* embryo (*3*, *4*). Ncd has been implicated in spindle function because of its cellular localization, the effects of *Ncd* mutations, and its slow, minus-end-directed microtubule-based motility in vitro (*3*−*8*).

Comparative studies between Ncd and kinesin are intriguing because there is remarkable structural similarity in their motor domains (*9*−*11*), yet these proteins exhibit dramatically different motility characteristics and in vivo functions (*11*, *12*). Kinesin is a plus-end-directed microtubule-based motor, and it drives the movement of neuronal membranous organelles toward the synapse. In the in vitro motility assays, kinesin promotes movements at rates 5−10 times faster than Ncd, and kinesin is processive for both motility and ATP turnover (*13*−*16*). These characteristics for kinesin are consistent with its role in axoplasmic transport. In contrast, Ncd is not processive for motility or ATP turnover (*17*−*20*), yet the motor domains of dimeric Ncd are cooperative (*21*). The slow, minus-end-directed microtubule movement of Ncd at 0.16 μm/s (*18*) is consistent with its involvement in spindle assembly. It is believed to cross-link microtubules and move to their minus-ends to focus the microtubule ends into the spindle poles (*4*, *22*).

The present models (*14*−*16*, *23*) to account for kinesin-promoted motility all encompass the original hand-over-hand hypothesis proposed by Hackney (*24*). The ATPase mechanism for processivity requires cooperative interactions between the motor domains of the kinesin dimer, and our understanding of these interactions is due in part to analysis of monomeric constructs (*16*, *23*, *25*−*29*).

Foster et al. (*21*) have shown cooperative interactions occur in the Ncd dimer, and this communication between the motor domains is believed to be important for Ncd to fulfill its role in spindle assembly and integrity. Crystal structures of both dimeric kinesin and Ncd have recently been published (*30*, *31*), and these results indicate that there are distinct differences in the neck domains upon dimerization that can account for the direction of movement (*31*). We anticipate that the structural differences detected in the Ncd and kinesin dimers will also lead to mechanistic differences in ATP turnover and force generation.

The approach that was undertaken in this study to understand the role of these cooperative interactions was to define the ATPase pathway for MC6, a monomeric construct of Ncd, and compare it to the dimeric MC1 (*20*, *32*). Several other groups have published kinetic models for monomeric

† This work was supported by Grant GM 54141 to S.P.G. from the National Institutes of Health, by Grant IRG-58-35 from the American Cancer Society, and in part by a Basil O'Connor Starter Scholar Research Award (5-FY95-1136) from the March of Dimes Birth Defects Foundation. S.P.G. is also the recipient of an American Cancer Society Junior Faculty Research Award (JFRA-618).

* To whom correspondence should be addressed at the Department of Biological Sciences, 518 Langley Hall, University of Pittsburgh, Pittsburgh, PA 15260. TEL.: (412) 624-5842. FAX: (412) 624-4759. Email: spg1+@pitt.edu.

[1] Abbreviations: Ncd, nonclaret disjunctional; MC1, Ncd construct of Leu^{209}−Lys^{700} amino acid residues; MC6, Ncd construct of Met^{333}−Lys^{700} amino acid residues; HEPES, *N*-(2-hydroxyethyl)piperazine-*N*′-2-ethanesulfonic acid; Mt·N and M·N in Schemes 1 and 2, microtubule·Ncd complex; DTT, dithiothreitol; mantADP, 2′(3′)-*O*-(*N*-methylanthraniloyl)adenosine 5′-diphosphate; mantATP, 2′(3′)-*O*-(*N*-methylanthraniloyl)adenosine 5′-triphosphate; 3′-dATP, cordycepin 5′-triphosphate; 2′-dATP, 2′-deoxyadenosine 5′-triphosphate; Kacetate, potassium acetate; MgAcetate, magnesium acetate; P_i, inorganic phosphate.

10.1021/bi991918+ CCC: $19.00
Published on Web 01/11/2000

Ncd (*33*−*35*), but the issue of cooperativity between the motor domains was not addressed in detail.

Our results show that there are differences in MC1 and MC6, but the most striking is in ATP-promoted dissociation. Dissociation from the microtubule is critical for the function of a molecular motor. Although MC1 can readily dissociate from the microtubule in an ATP-dependent manner, MC6 appears to remain on the microtubule for several cycles of ATP turnover. These results imply that the partner motor domain is required for ATP-dependent detachment of Ncd from the microtubule.

EXPERIMENTAL PROCEDURES

Materials. [α-^{32}P]ATP (>3000 Ci/mmol) was purchased from NEN Life Science Products, PEI-cellulose F TLC plates (EM Science of Merck, 20 × 20 cm, plastic-backed) were from VWR Scientific (West Chester, PA), and taxol (*Taxus brevifolia*) was from Calbiochem. ATP, GTP, and SP-Sepharose were obtained from Pharmacia Biotech Inc. (Upsala, Sweden).

Buffer Conditions. The kinetic and equilibrium binding experiments were performed at 25 °C in ATPase buffer (50 mM HEPES, pH 7.2, with KOH, 5 mM MgAcetate, 0.1 mM EDTA, 0.1 mM EGTA, 50 mM KAcetate, 1 mM DTT, and 5% sucrose).

Protein Purification. Monomeric MC6 and dimeric MC1 were expressed from plasmids pET/MC6 and pET/MC1, respectively (*32*), and these clones were generously provided by Dr. Sharyn Endow, Duke University Medical Center. MC6 and MC1 were expressed in *Escherichia coli* strain BL21(DE3) and purified as described previously (*21*). Microtubules were assembled with 20 μM taxol from soluble, purified tubulin (cold-depolymerized and clarified the morning of each experiment). The microtubules were collected by centrifugation, and the microtubule pellet was resuspended in ATPase buffer plus 20 μM taxol to stabilize the microtubules (*36*). For all the experiments in which microtubules were present, there was also 20 μM taxol present to maintain the polymer state of the microtubules.

Active Site Titration. There is a significant discrepancy between the concentration of MC6 determined spectrophotometrically based on the absorbance at 280 nm relative to the absorbance at 259 nm which evaluates ADP concentration (*21*). A_{259} has been used to determine Ncd site concentration because Ncd is purified with ADP tightly bound at the active site (*21*, *35*). Furthermore, the determination of MC6 protein concentration by the BioRad Protein Assay (ovalbumin as standard) agrees with the A_{280} determination, but the site concentration based on the A_{259} determination is significantly higher. To determine the active site concentration of MC6 protein, a phosphocreatine kinase coupled assay was used (*25*). In the presence of the phosphocreatine kinase ATP regeneration system, accessible ADP free in solution is converted to ATP; therefore, ADP at the active site of MC6 is inaccessible and can be quantified as the concentration of MC6 active sites. To begin the assay, MC6 was incubated with radiolabeled [α-^{32}P]ATP for 90 min to allow for ADP release and the binding and turnover of [α-^{32}P]ATP at the active site of the enzyme. The reaction volume of this initial step was 50 μL with a trace amount of radiolabeled nucleotide present (5 μL) and MC6 at a concentration of 40 μM based on the Bradford estimate. After the 90 min incubation, the reaction volume was increased to 200 μL by adding 150 μL of ATPase buffer (Reaction Mix A), resulting in a concentration of 10 μM for MC6; 100 μL of Reaction Mix A was used for the assay in the absence of ATP, and the second 100 μL aliquot was used for the assay in the presence of MgATP. Reaction Mix B contained phosphocreatine kinase (0.30 mg/mL), 4 mM phosphocreatine, ±5 mM MgATP in ATPase buffer. Five microliters of Reaction Mix A was pipetted rapidly with 5 μL of Reaction Mix B and incubated for times varying from 5 s to 20 min. After mixing, the final concentration of reactants was 5 μM MC6, 0.15 mg/mL phosphocreatine kinase, 2 mM phosphocreatine, ±2.5 mM MgATP. The reaction was terminated by the addition of 10 μL of 2 N HCl, followed by 20 μL of chloroform to degrade the protein. The reaction mixtures were neutralized with 2 M Tris/3 M NaOH (∼5 μL) to pH ∼7.2−8.0 for ADP and P_i separation from ATP by thin-layer chromatography. An aliquot (1.5 μL) of each reaction mixture was spotted on a PEI−cellulose TLC plate and subsequently developed with 0.6 M potassium phosphate buffer, pH 3.4, with phosphoric acid. Radiolabeled nucleotide was quantified using a FUJI Bas-2000 PhosphorImager (Fuji Photo Film Co., Ltd.), and the data were analyzed using KaleidaGraph software (Synergy Software, Reading, PA). The data were fit to eq 1:

$$[\mathrm{ADP}] = A\exp(-k_1 t) + C \qquad (1)$$

where the active site concentration is the sum of the amplitude (*A*) and the constant term (*C*) to extrapolate to zero time and *t* is time in seconds. In the experiment with excess nonradioactive MgATP (2.5 mM), k_1 is the first-order rate constant for ADP release in the absence of microtubules.

The active site concentration determined in the presence of the ATP chase was equivalent to the active site concentration determined in the absence of ATP. To ensure the coupled assay was fast enough to regenerate ATP, control experiments were performed with double (0.3 mg/mL final concentration after mixing) and triple (0.45 mg/mL) amounts of the phosphocreatine kinase. No difference was observed in the kinetics at 0.15−0.45 mg/mL phosphocreatine kinase.

Steady-State ATPase Kinetics. Steady-state ATPase measurements were determined by following the hydrolysis of [α-^{32}P]ATP to form [α-^{32}P]ADP·P_i as described previously (*36*).

Microtubule Equilibrium Binding Experiments. These experiments were performed as described previously (*21*). All concentrations reported are final after mixing. 2 μM MC6 was incubated with microtubules (0−7 μM) in the absence of any added nucleotide for 30 min and then centrifuged as described previously. The supernatant was removed, and 5× Laemmli sample buffer was added. The microtubule pellet was washed with ATPase buffer + 20 μM taxol and resuspended in 5× Laemmli sample buffer plus 220 μL of ATPase buffer. The samples were boiled for 5 min and then loaded onto an 8% acrylamide, 2 M urea SDS gel and electrophoresed. The gel was then stained with Coomassie Blue, analyzed by a Microtek ScanMaker X6EL scanner (Microtek, Redondo Beach, CA), and quantified using NIH Image version 1.60 to determine the concentration of MC6 in the supernatants and pellets at each microtubule concen-

tration. Fractional binding, defined as the ratio of sedimented MC6 to total MC6, is presented in Figure 3 as a function of microtubule concentration. The data were fit to the quadratic equation:

$$[\mathrm{Mt{\cdot}N}]/[\mathrm{N_0}] = 0.5\{([\mathrm{N_0}] + [\mathrm{Mt_0}] + K_\mathrm{d}) - [([\mathrm{N_0}] + [\mathrm{Mt_0}] + K_\mathrm{d})^2 - 4([\mathrm{N_0}][\mathrm{Mt_0}])]^{1/2}\} \quad (2)$$

where Mt·N is the fraction of MC6 sedimenting with the microtubule pellet, N_0 is the total MC6 concentration, Mt_0 is the total tubulin concentration, and K_d is the dissociation constant.

Rapid Quench Experiments. The pre-steady-state kinetic experiments to determine the rate constant for ATP hydrolysis were performed with a rapid chemical quench-flow instrument (Kintek Corp., Austin, TX) at 25 °C in ATPase buffer. MC6 and taxol-stabilized microtubules were preincubated for 15 min to form the Mt·MC6 complex and then reacted with [α-^{32}P]ATP for times ranging from 5 ms to 5 s. The reaction was then quenched with 2 N HCl and expelled from the instrument. Chloroform (100 μL) was added immediately to the reaction mixture to denature the protein. This procedure was followed by neutralization with 2 M Tris/3 M NaOH to pH 7.2−8.0 for analysis by TLC. The acid quench experiments determined the time course of ATP hydrolysis and the formation of the acid-labile products ADP and P_i at the active site of the enzyme. Therefore, the product formed for each time point represents the sum of MC6·[α-^{32}P]ADP·P_i, MC6·[α-^{32}P]ADP, and [α-^{32}P]ADP released from the active site and free in solution. The data were fit to the burst equation:

$$\text{Product} = A[1 - \exp(-k_\mathrm{b}t)] + k_2t \quad (3)$$

where A is the amplitude of the burst, which represents the formation of [α-^{32}P]ADP·P_i on the active site; k_b is the rate constant of the pre-steady-state burst phase; t is time in seconds; and k_2 is the rate constant of the linear phase and corresponds to steady-state turnover.

Stopped-Flow Experiments. The pre-steady-state kinetics of mantATP binding, mantADP binding, mantADP release, MC6 binding to microtubules, and detachment of MC6 from microtubules were measured using an SF-2001 KinTek stopped-flow instrument at 25 °C in ATPase buffer. The preparation, purification, and characterization of the *N*-methylanthraniloyladenosine nucleotides used in this study were described previously (*23*, *37*, *38*). For the experiments with these analogues, excitation was at 360 nm (Hg arc lamp) with emitted light monitored through a 400 nm cutoff filter. The mantADP and mantATP binding data in Figures 6B and 7B, respectively, were fit to the following equation:

$$k_\mathrm{obs} = k_\mathrm{on}[\mathrm{mantAXP}] + k_\mathrm{off} \quad (4)$$

where k_{obs} is the rate constant obtained from the exponential phase of the fluorescence change, k_{on} defines the second-order rate constant for mantADP or mantATP binding, and k_{off} corresponds to the observed rate constant of mantADP or mantATP release, as determined by the *y*-intercept. The dissociation kinetics of the Mt·MC6 complex and the kinetics of microtubule binding by MC6 were determined by the change in turbidity monitored at 340 nm. All concentrations reported are final after mixing. The equilibrium constants for microtubule binding, mantADP binding, and mantATP binding were defined by eq 5:

Scheme 1: Microtubule·Ncd (M·N) ATPase Mechanism

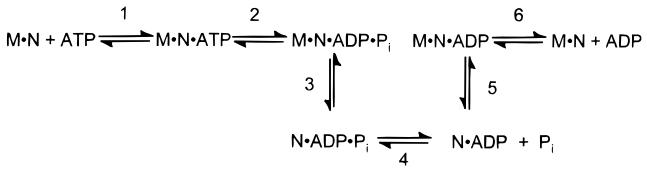

$$K_\mathrm{d} = k_\mathrm{off}/k_\mathrm{on} \quad (5)$$

Data Analysis. In addition to conventional data fitting, the kinetic data were also modeled using the KINSIM kinetic simulation program (*39*). The kinetics were simulated using Scheme 2, and the constants presented in Scheme 2 represent the best fit of all the data to the single mechanism (steps 1−6). The acid-quench transients were modeled by acid output = [N·ADP·P_i] + [ADP]. The mantADP release kinetics were modeled based on the assumption that mantADP would not rebind to MC6 once released from the active site because of the high concentration of MgATP present in the microtubule syringe (Figure 5). The partitioning of the Mt·N·mantADP intermediate was considered because the steady-state $K_{1/2,Mt}$ equals 9.6 μM and the observation of a significant k_{-5} in the microtubule binding experiments (Figure 4). These experiments indicated that the initial collision of the MC6 motor with the microtubule may not lead to mantADP release, and the KINSIM simulations tested this hypothesis.

$$\text{mantADP output} = \mathrm{X1}([\mathrm{Mt{\cdot}N{\cdot}mantADP}] + [\mathrm{N{\cdot}mantADP}])$$

The partitioning factor X1 represents the fraction of Mt·N·mantADP that proceeds toward release of mantADP to form the Mt·N intermediate with

$$\mathrm{X1} = k_{+6}/(k_{-5} + k_{+6})$$

RESULTS

The objective of this study was to define the pathway of ATP hydrolysis for monomeric Ncd and to identify the steps in the ATPase cycle where cooperativity between the two motor domains may be occurring. Scheme 1 is a minimal mechanism based on our MC1 and MC6 equilibrium binding studies (*21*), and this scheme served as our model for the design of the pre-steady-state kinetic experiments presented. All steps in Scheme 1 were measured directly for monomeric MC6 except inorganic phosphate release (k_{+4}).

Active Site Titration. One of the hallmarks of kinesin superfamily members is the tight binding of ADP at the active site in the absence of microtubules (*35*, *40*). This tight affinity for ADP was exploited to determine the concentration of active enzyme in each preparation of MC6 (Figure 1). Radiolabeled ATP ([α-^{32}P]ATP) was added to MC6 and allowed to incubate for 90 min. During this time frame, all of the radiolabeled ATP present was hydrolyzed to [α-^{32}P]-ADP + P_i (data not shown). After the incubation, a chase solution containing creatine kinase plus phosphocreatine was added to the enzyme mixture. ADP released from the active

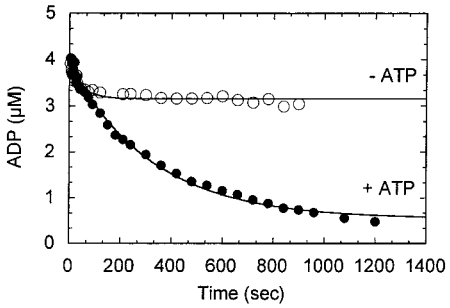

FIGURE 1: MC6 active site determination and ADP release in the absence of microtubules. The MC6·[α-^{32}P]ADP complex (5 μM MC6) was rapidly mixed with 0.30 mg/mL creatine kinase, 4 mM phosphocreatine in the absence (○) or in the presence (●) of 5 mM MgATP at 25 °C. All concentrations reported are final concentrations after mixing. The data were fit to eq 1, [ADP] = A exp($-k_1t$) + C, where the sum of the amplitude (A) and the constant term (C) is equal to the ADP concentration at time 0. This sum represents the total MC6 enzyme sites that bind [α-^{32}P]ADP tightly to form the MC6·ADP intermediate and provides the active site concentration at 4.1 ± 0.1 μM. In the presence of unlabeled MgATP (●), the rate of [α-^{32}P]ADP release (k_1) was determined to be 0.003 ± 0.0006 s^{-1}. All experiments were performed in ATPase buffer (50 mM HEPES, pH 7.2 with KOH, 5 mM MgAcetate, 0.1 mM EDTA, 0.1 mM EGTA, 50 mM KAcetate, 1 mM DTT, and 5% sucrose) at 25 °C.

site of MC6 would be converted to ATP by the phosphoryl group transfer reaction catalyzed by creatine kinase. Therefore, the only radiolabeled ADP remaining after incubation with the chase solution is [α-^{32}P]ADP tightly bound to MC6 and inaccessible to the creatine kinase−phosphocreatine coupled assay. The chase reaction was also performed in the presence of 2.5 mM MgATP. Under these conditions, there is a greater probability that MC6 will bind an unlabeled ATP rather than [α-^{32}P]ATP regenerated by creatine kinase. Thus, the chase in the presence of 5 mM ATP permits the determination of the rate constant for [α-^{32}P]ADP release from the active site in the absence of microtubules. Figure 1 shows the results for one MC6 preparation with the active site concentration at 4.1 μM. Three MC6 preparations were used for the experiments presented here, and all concentrations reported represent the concentration of MC6 active sites based on this assay.

In the ATP chase experiment (Figure 1), the rate constant for ADP release in the absence of microtubules at 0.003 s^{-1} is comparable to the rate of steady-state turnover in the absence of microtubules (k_{cat} = 0.004 ± 0.0002 s^{-1}). These rates are also comparable to the observed rate constant for mantADP release (k_{obs} = 0.005 ± 0.0006 s^{-1}) from the MC6·mantADP complex measured in the stopped-flow instrument (Figure 5B). These results show that ADP is tightly bound to monomeric MC6 in the absence of microtubules. Furthermore, the kinetics of mantADP release indicate that this fluorescent ADP analogue is also tightly bound to the active site of MC6 comparable to ADP. The data indicate that mantADP is a good analogue for MC6, consistent with results reported for other monomeric and dimeric constructs of Ncd (*20*, *33*−*35*).

Steady-State ATP Hydrolysis. Our steady-state results (Figure 2) revealed that the slow turnover of ATP was dramatically stimulated by microtubules, a characteristic common for both monomeric and dimeric kinesin superfamily members (*25*, *26*, *35*, *40*). Figure 2A shows the

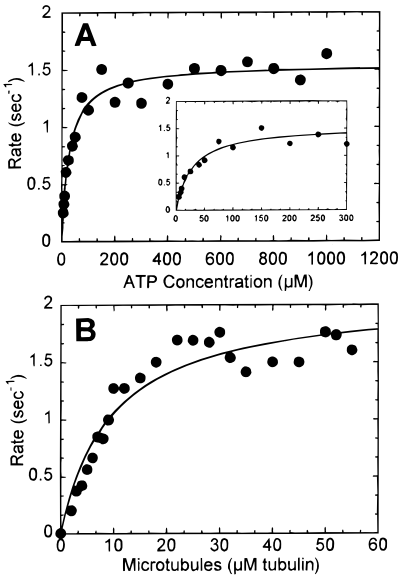

FIGURE 2: Steady-state ATP hydrolysis of MC6. (A) The Mt·MC6 complex (1 μM MC6 plus taxol-stabilized microtubules at 50 μM tubulin) was preformed and incubated with MgATP (0−1 mM) in ATPase buffer at 25 °C. The rate of [α-^{32}P]ATP hydrolysis is shown as a function of ATP concentration. The fit of the data to a hyperbola provided the k_{cat} = 1.6 ± 0.04 s^{-1} and the $K_{m,ATP}$ = 28.3 ± 3.7 μM. The inset shows the initial part of the curve, 0−300 μM MgATP. (B) The Mt·MC6 complex was preformed with 1 μM MC6 plus taxol-stabilized microtubules (0−55 μM tubulin) and incubated with 1 mM MgATP. The data show the rate of [α-^{32}P]-ATP hydrolysis as a function of microtubule concentration. In the absence of microtubules, the steady-state rate constant of ATP turnover is 0.004 ± 0.0002 s^{-1}. The fit of the data to a hyperbola yields k_{cat} = 2.1 ± 0.11 s^{-1}; $K_{1/2,Mt}$ = 9.6 ± 1.6 μM.

kinetics at 50 μM tubulin and as a function of ATP concentration: k_{cat} = 1.6 s^{-1}, $K_{m,ATP}$ = 28 μM. Figure 2B presents the kinetics at 1 mM MgATP as a function of microtubule concentration. Note that the rate of steady-state turnover increased from 0.004 s^{-1} in the absence of microtubules to 2.1 s^{-1} obtained from the fit of the data to a hyperbola with the $K_{1/2,Mt}$ = 9.6 μM. A different k_{cat} parameter is obtained by the two experiments (Figure 2A and Figure 2B) because a nonsaturating concentration of microtubules was used in the ATP-dependent steady-state experiment (Figure 2A). The experiment presented in panel A was performed at 50 μM tubulin, and the k_{cat} based on this experiment was 1.6 s^{-1}. Note that the ATPase rate at 50 μM tubulin in Figure 2B is also 1.6 s^{-1}. Experiments at microtubule concentrations >50 μM tubulin are difficult to interpret because of the increased viscosity of the microtubule·MC6 solution; accurate pipetting and mixing become problematic. Our reported k_{cat} for MC6 is based on the hyperbolic fit of the data from the microtubule concentration dependence because it provides a better representation of the maximum rate of ATP turnover at saturating microtubules and ATP. The variability of steady-state kinetic parameters among three preparations used in the experiments presented here is not very large: k_{cat} = 1.90 ± 0.10 s^{-1}, $K_{M,ATP}$ = 27.8 ± 10.9 μM (12−35 μM), $K_{1/2,Mt}$ = 9.6 ± 3.9 μM (6−14 μM).

Equilibrium Binding of MC6 to the Microtubule. To determine the relative affinity of MC6 for microtubules, equilibrium binding experiments were pursued as a function of microtubule concentration and in the absence of added nucleotides or nucleotide analogues. The Mt·MC6 complexes

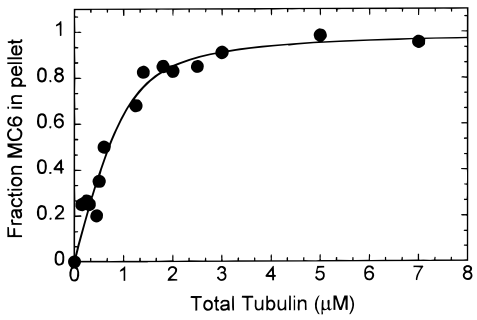

FIGURE 3: Equilibrium binding of MC6 to microtubules. MC6 at 2 μM was incubated with microtubules (0−7 μM tubulin) for 30 min in the absence of added nucleotide as described under Experimental Procedures. The fraction of MC6 sedimenting in the microtubule pellet was plotted as a function of the total microtubule concentration. The fit of the data to the quadratic equation (eq 2) yields the apparent $K_{d,Mt}$ = 0.20 ± 0.06 μM with maximum fractional binding at 1.0 ± 0.05.

were incubated for 30 min to reach equilibrium and then centrifuged to obtain the supernatant and pellet for each Mt·MC6 reaction. MC6 and tubulin were separated by SDS−polyacrylamide gel electrophoresis, the gel was stained with Coomassie Blue and analyzed using NIH Image 1.60. Figure 3 shows that MC6 partitioned with microtubules as a function of tubulin concentration. The fit of these data to the quadratic equation (eq 2) provided the apparent $K_{d,Mt}$ at 0.2 μM tubulin. This constant for monomeric MC6 is equivalent to the $K_{d,Mt}$ for MC1 reported at 0.22 μM (*21*), suggesting that monomeric MC6 binds to microtubules as tightly as dimeric MC1 in the absence of added nucleotides or nucleotide analogues. Fractional binding reached 100%, consistent with MC6 remaining stable and fully active during the assay. The observation that the microtubule binding constants for MC1 and MC6 were equivalent also supports the model that the Ncd dimer binds to the microtubule with one motor domain bound and the other detached and positioned toward the minus-end of the microtubule poised for binding to the next site on the microtubule (*42*−*44*).

Pre-Steady-State Kinetics of MC6·ADP Binding to the Microtubule. We assumed that MC6·ADP is the intermediate that binds to microtubules during the ATPase cycle because MC6 is purified with ADP bound at the active site. To measure the formation of the Mt·MC6·ADP complex, MC6 as purified was rapidly mixed with taxol-stabilized microtubules and a change in turbidity was monitored in the stopped-flow instrument. Figure 4A illustrates the exponential increase in turbidity as a function of time. Figure 4B shows that the observed rate of binding increased linearly as a function of microtubule concentration. The slope of the line provided the second-order rate constant for binding (k_{+5} = 0.77 μM^{-1} s^{-1}) and the *y*-intercept (k_{-5} = 3.6 s^{-1}). These data yield an apparent $K_{d,Mt}$ = 4.7 μM tubulin as determined using eq 5.

Pre-Steady-State Kinetics of MantADP Release from the Mt·MC6·MantADP Complex. MC6 was incubated with a fluorescent analogue of ADP, mantADP, at a 1:2 ratio to exchange the ADP at the active site with mantADP. The preformed MC6·mantADP complex was rapidly mixed with microtubules plus MgATP in the stopped-flow instrument, and the exponential decrease in fluorescence was observed as a function of time. The MgATP, included in the microtubule syringe, blocked the subsequent rebinding of

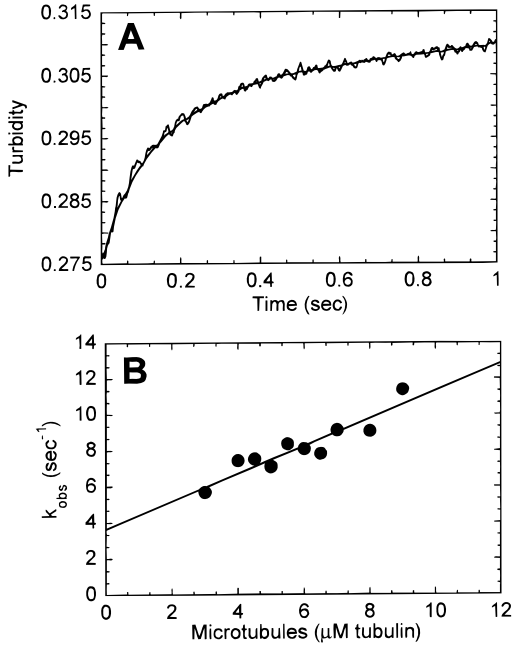

FIGURE 4: Pre-steady-state kinetics of MC6·ADP binding to the microtubule. All concentrations reported are final after mixing in the stopped-flow instrument. (A) MC6 at 4 μM was reacted with taxol-stabilized microtubules (6.5 μM tubulin), and the change in turbidity was monitored. The stopped-flow transient (jagged line) represents the average of 6 individual stopped-flow traces. The smooth line is the fit of the data to a single-exponential function with a linear term. The observed rate constant of the fast exponential phase was 7.9 ± 0.1 s^{-1}. (B) The observed exponential rate constant increased linearly with increasing microtubules. The slope provides the second-order rate constant for microtubule binding, k_{+5} = 0.77 ± 0.11 μM^{-1} s^{-1}, and the *y*-intercept, k_{-5} = 3.6 ± 0.6 s^{-1}.

mantADP to MC6 once it was released from the active site. Figure 5 shows that the exponential rate constant associated with the fluorescence change upon mantADP release increased with increasing microtubule concentration. The fit of the data to a hyperbola provides the maximum rate constant of mantADP release, k_{+6} = 3.9 s^{-1}. ADP release has been reported as the rate-limiting step for steady-state turnover for both dimeric and monomeric constructs of Ncd (*21*, *33*−*35*). However, there is a significant difference between the k_{cat} for MC6 at 1.9 s^{-1} and the first-order rate constant for mantADP release at 3.9 s^{-1}. We pursued experiments to resolve this possible discrepancy between the steady-state k_{cat} and the observed mantADP release rate constant.

Pre-Steady-State Kinetics of MantADP Binding to the Mt·MC6 Complex. One hypothesis to account for the discrepancy in the pre-steady-state and steady-state kinetics is that the release of mantADP may be reversible such that steady-state turnover is limited by partitioning of the Mt·MC6 intermediate between mantADP rebinding and ATP binding (Mt·N·ADP ⇄ Mt·N ⇄ Mt·N·ATP). To test this possibility, a preformed Mt·MC6 complex (10 μM MC6, 20 μM tubulin) was rapidly mixed in the stopped-flow instrument with varying concentrations of mantADP. Figure 6A shows a representative experiment at 45 μM mantADP and displays the increase in fluorescence associated with mantADP binding to the more hydrophobic active site of MC6. The exponential rate constant of the fluorescence change increased linearly as a function of mantADP concentration as shown in Figure 6B. The fit of the data to eq 4 provided the

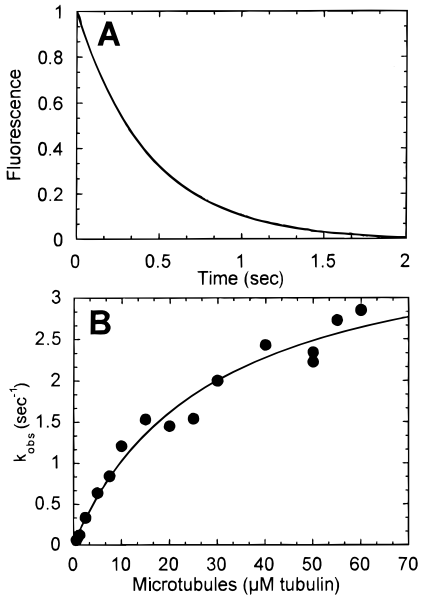

FIGURE 5: Pre-steady-state kinetics of mantADP release from Mt·MC6·mantADP complex. (A) A representative stopped-flow record of the change in fluorescence due to the release of mantADP from the Mt·MC6·mantADP complex. The preformed MC6·mantADP complex (2 μM MC6 + 4 μM mantADP) was rapidly mixed with taxol-stabilized microtubules (50 μM tubulin, 20 μM taxol, plus 1 mM MgATP). The jagged line represents the fluorescence signal (average of 5 stopped-flow traces), and the smooth line is the fit of the data to a single-exponential function (k_{obs} = 2.22 ± 0.002 s^{-1}). (B) The observed exponential rate constants of the fluorescence decrease were plotted as a function of microtubule concentration. The data were fit to a hyperbola where the maximum rate constant of mantADP release was 3.9 ± 0.35 s^{-1}.

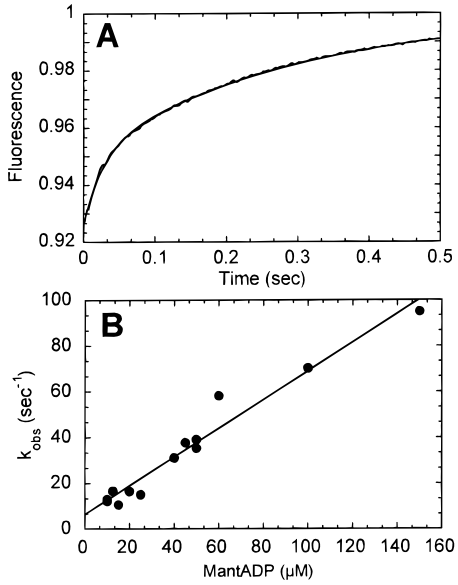

FIGURE 6: Pre-steady-state kinetics of mantADP binding to the Mt·MC6 complex. (A) A preformed Mt·MC6 complex (5 μM MC6, 10 μM tubulin, 20 μM taxol) was rapidly mixed with 45 μM mantADP. An increase in fluorescence was observed (jagged line, average of 6 individual stopped-flow traces) and fit to two exponential functions (smooth line). The observed rate of the first phase at 45 μM mantADP was 37.7 ± 0.9 s^{-1}. The slow phase (3.5 ± 0.02 s^{-1}) may represent mantADP binding to sites that were initially occupied by ADP such that mantADP binding to these sites was limited by ADP release. (B) The observed rate constants of the fast exponential increase were plotted as a function of mantADP concentration (10−150 μM). The data were fit to eq 4. The slope of the line provides the second-order rate constant for mantADP binding, k_{-6} = 0.6 ± 0.04 μM^{-1} s^{-1}, and k_{+6} at 6.4 ± 2.3 s^{-1} was obtained from the *y*-intercept.

second-order rate constant of mantADP binding, k_{-6} = 0.6 μM^{-1} s^{-1}. The k_{+6}, obtained from the *y*-intercept, was 6.4 ± 2.3 s^{-1}. This off rate is somewhat higher than 3.9 s^{-1} determined by direct measurement of mantADP release presented in Figure 5, but the rate constant obtained from the *y*-intercept is less accurate than the direct measurement in Figure 5. The mantADP binding experiment does provide evidence that step 6 is reversible. Further evidence of the reversibility of this step came from mantADP release experiments comparable to those presented in Figure 5. ATP or ADP was added with the microtubules to block rebinding of mantADP. The experiments were performed as a function of ATP or ADP concentration. The observation was that the amplitude of the fluorescence change associated with mantADP release increased as a function of ATP or ADP concentration, indicative that the amplitude of the fluorescence change was affected by rebinding of mantADP (data not shown). The results from these experiments and the mantADP binding experiments presented in Figure 6 indicate that ADP release is a reversible step for monomeric MC6.

MantATP Binding to the Mt·MC6 Complex. Figure 7A presents the kinetics of mantATP binding to the Mt·MC6 complex (8 μM MC6, 20 μM tubulin). There is an exponential increase in fluorescence associated with mantATP binding to the more hydrophobic environment of the active site of the enzyme, and the rate of the observed fluorescence change increases as a function of mantATP concentration. The fit of the data to eq 4 provided the second-order rate constant of mantATP binding, k_{+1} = 1.06 μM^{-1} s^{-1}. Experiments were also performed with 2′mant-3′dATP and 3′mant-2′dATP, and the results are presented in Table 1. The results show that the kinetics of mantATP binding were similar for the 2′mant-3′dATP derivative and the mantATP mixture, yet the 3′mant-2′dATP derivative displayed a 5-fold higher *y*-intercept. The *y*-intercept for the mantATP binding experiments reflects the composite rate constant of all reactions which lead to release of mant nucleotide (k_{-1} and k_{+6}). These results suggest that 3′mant-2′dATP binding was much weaker than either 2′mant-3′dATP or mantATP binding. With dimeric MC1, the 3′mant-2′dATP derivative also showed much weaker binding than either 2′mant-3′dATP or mantATP (*20*). The dimeric MC1 binding kinetics of mantATP exhibited no significant off rate, suggesting that ATP binding was tighter (*20*).

ATP Hydrolysis by the Mt·MC6 Complex. A preformed Mt·MC6 complex (10 μM MC6, 30 μM tubulin) was rapidly mixed in the rapid quench instrument with 300 μM [α-^{32}P]-ATP, and the time dependence of ATP hydrolysis was determined (Figure 8). The results show that there was a burst of ADP + P_i formed at the active site during the first ATP turnover, and this exponential rate constant k_b = 11 s^{-1}. The burst rate did not increase appreciably at ATP concentrations >150 μM (150−500 μM ATP), indicating that ATP binding is faster than ATP hydrolysis. Therefore, the burst rate at 300 μM ATP represents the rate constant for ATP hydrolysis, k_{+2} = 11 s^{-1}. The amplitude of the burst at 10.4 ± 1.5 μM was equivalent to the concentration of enzyme sites (10 μM) within experimental error. This result indicates that our estimation of active sites of MC6 based

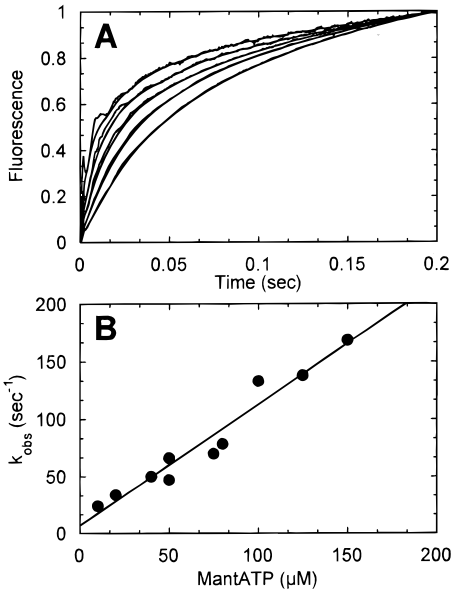

FIGURE 7: MantATP binding to the Mt·MC6 complex. MantATP was rapidly mixed in the stopped-flow instrument with a preformed Mt·MC6 complex (8 μM MC6, 20 μM tubulin, 20 μM taxol). (A) Transients are shown for the following concentrations of mantATP: 10, 20, 40, 100, 150 μM (from the bottom to the top trace). Fluorescence signals were normalized to show the relative change in fluorescence for each mantATP concentration on a single graph; the smooth lines represent the fit of the data to an exponential function plus a linear term. (B) The observed exponential rate constant was plotted as a function of mantATP concentration. The data were fit to eq 4 which yields the second-order rate constant for mantATP binding, $k_{+1} = 1.06 \pm 0.09$ μM^{-1} s^{-1}, and the y-intercept, 6.9 ± 7.3 s^{-1}. Panel B includes additional data that are not shown in panel A.

Table 1: MantATP Binding Constants

substrate	k_{+1} (μM^{-1} s^{-1})	k_{-1} (s^{-1})	$K_{d,app}$ (μM)
mantATP	1.06 ± 0.09	6.9 ± 7.3	
2′mant-3′dATP	0.77 ± 0.07	5.2 ± 5.7	
3′mant-2′dATP	1.40 ± 0.12	26.7 ± 4.8	19.1
mantADP	0.63 ± 0.04	6.4 ± 2.3	10.2

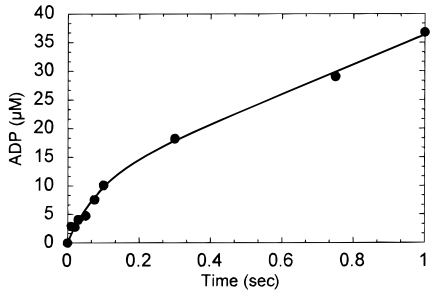

FIGURE 8: Pre-steady-state ATP hydrolysis by the Mt·MC6 complex. MgATP at 300 μM was rapidly mixed with a preformed Mt·MC6 complex (10 μM MC6, 30 μM tubulin) in the rapid quench instrument and allowed to react for 0.01−1 s, followed by the HCl acid quench. The data were fit to the burst equation (eq 3) where the amplitude of the burst $A = 10.4 \pm 1.5$ μM, the rate constant of the burst phase $k_b = 11.3 \pm 2.6$ s^{-1}, and rate constant of the linear phase $k_{ss} = 25.8 \pm 1.9$ μM·s^{-1} or 2.6 s^{-1} per MC6 site.

on the phosphocreatine kinase coupled assay (Figure 1) is an accurate method of active site determination. The results also suggest that the microtubules fully activated ADP release from MC6; however, other experiments imply that there is an equilibrium occurring (Mt·MC6 ⇄ Mt·MC6·ADP) because the observation of full burst amplitude did vary between experiments. We pursued experiments to remove the ADP at the active site of MC6 by pretreatment of the Mt·MC6·ADP complex with apyrase to convert ADP to AMP in the reaction mixture (*33*). The kinetics with the apyrase-treated Mt·MC6 complex were consistent with the data in Figure 8 although the amplitude was reduced because of the decreased stability of MC6 in the absence of nucleotide (*33*, *45*). The rate constant of the linear phase in the acid-quench experiment correlates well with the steady-state rate determined directly.

ATP-Induced Dissociation Kinetics of the Mt·MC6 Complex. The traditional experiment to measure motor detachment from its cytoskeletal partner is to observe a change in the light scattering or turbidity signal associated with detachment of the motor from the filament as a function of ATP concentration (*46*). Figure 9 presents these experimental results for the Mt·MC6 complex. Figure 9A shows a representative stopped-flow record where 15 μM MgATP was rapidly mixed with a Mt·MC6 complex (2 μM MC6, 2 μM tubulin), and a change in turbidity was measured. The fit of the data to a single-exponential plus a linear term provides the k_{obs} of the fast exponential reaction at 6.5 s^{-1}. The rate of the fast exponential phase increased as a function of ATP concentration, and the fit of the data to a hyperbola yielded the maximum rate constant of the ATP-dependent process at 14 s^{-1} with the $K_{1/2,ATP}$ at 20 μM (Figure 9B). In the absence of ATP (buffer alone), only a flat noisy signal was observed with no definitive decrease in turbidity (data not shown).

We designed an experiment to test the hypothesis that monomeric MC6 was not detaching from the microtubule, a hypothesis also proposed for monomeric kinesin based on kinetic and motility data (*26*−*28*, *47*, *48*). Figure 9C shows the experiment comparing the dissociation kinetics of dimeric MC1 with monomeric MC6. In this experiment, the Mt·Ncd complex with either 4 μM MC1 or 4 μM MC6 was rapidly mixed with 1 mM MgATP in the stopped-flow instrument. The rate constant of the exponential phase for dimeric MC1 at 14.4 s^{-1} was comparable to that of monomeric MC6 at 11.4 s^{-1}. However, the amplitude associated with the change in turbidity was dramatically different. MC1 showed a relative amplitude of 0.32 while the relative amplitude for MC6 was only 0.02. Therefore, the amplitude associated with MC6 dissociation was only 6% of the MC1 amplitude. We repeated the MC6 dissociation kinetics at 1 mM MgATP with increasing salt concentration (150−550 mM final concentration including buffer 50 mM KAcetate + KCl) and observed a progressive increase in the amplitude associated with the MC6 dissociation kinetics. The salt would act to weaken the affinity of MC6 for microtubules; therefore, at high salt conditions (1 mM MgATP + 550 mM salt), the MC6 amplitude approached that of dimeric MC1. These results show that the dramatic difference in the amplitude of the dissociation kinetics of MC6 and MC1 cannot be accounted for by a difference in the relative molecular weight of the two constructs (M_r 42 025 for MC6 vs 57 789 per motor domain for dimeric MC1) (*21*, *49*). Furthermore, the control microtubules in the absence of Ncd reacted at the high salt conditions (1 mM MgATP + 550 mM salt) showed no change in turbidity, indicative that the high salt was not leading to disassembly of microtubules and contributing to the turbidity signal observed for the Mt·MC6 kinetics at high

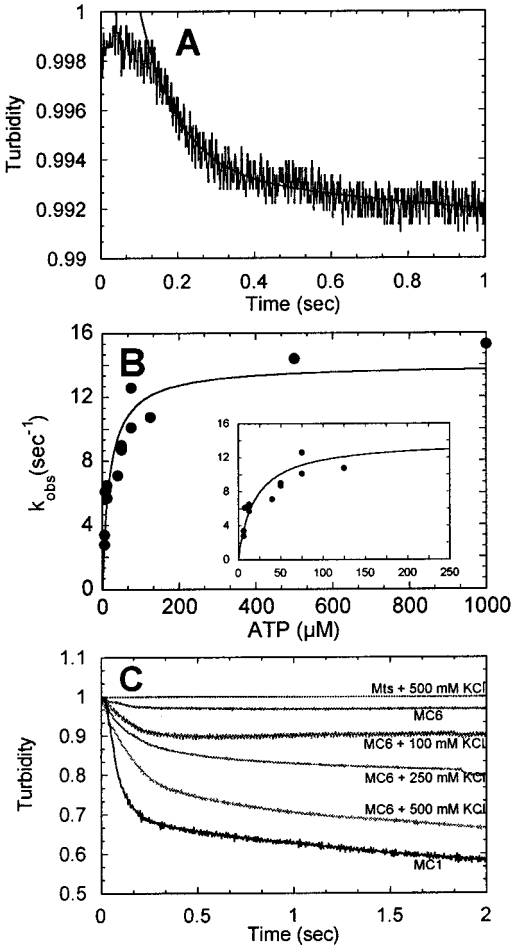

FIGURE 9: ATP-induced dissociation kinetics of the Mt·MC6 complex. (A) MgATP (15 μM + 100 mM KCl final concentration) was rapidly mixed with the preformed Mt·MC6 complex (2 μM MC6, 2 μM tubulin final) and monitored in a stopped-flow instrument to measure the kinetics of MC6 dissociation from the microtubule (average of 6 individual traces). The smooth line is the fit of the data to a single exponential providing $k_{obs} = 6.5 \pm 0.4$ s^{-1} at 15 μM ATP. (B) The observed exponential rate is plotted as a function of MgATP concentration. The data were fit to a hyperbola with $k_{+3} = 14.0 \pm 0.9$ s^{-1}. The $K_{1/2,ATP}$ for this experiment was 19.6 ± 4.5 μM. The inset shows the data for 0−250 μM MgATP. (C) The ATP-induced dissociation kinetics of dimeric MC1 were measured at the same time as the dissociation kinetics for monomeric MC6. Both Mt·Ncd complexes were preformed with either 4 μM MC6 or 4 μM MC1(active site concentrations) with microtubules at 6 μM tubulin, and the reactions were initiated with 1 mM MgATP plus KCl. All reactions were in ATPase buffer which contains 50 mM KAcetate in addition to any KCl added to the reaction. The data were fit to either one or two exponential terms. For MC1 in the absence of added KCl: $k_{obs} = 14.4 \pm 0.2$ s^{-1}; relative amplitude = 0.32 ± 0.004. MC6: $k_{obs} = 11.4 \pm 0.6$ s^{-1}; relative amplitude = 0.02 ± 0.001. Note that there is a progressive increase in the amplitude associated with MC6 dissociation kinetics as the added salt was increased from 0 to 500 mM KCl. There was no appreciable turbidity signal associated with the reaction in which microtubules (6 μM tubulin) in the absence of motor were reacted with 1 mM MgATP + 500 mM KCl.

salt. Based on the results presented in Figure 9, we propose that there is a small population of monomers that do dissociate from the microtubule at low salt conditions, and the relative amplitude associated with the kinetics of MC6 reflects this population. The alternative hypothesis to account for the turbidity signal is that it represents an ATP-dependent conformational change that occurs while MC6 is bound to the microtubule but the conformational change is uncoupled from ATP-dependent movement. This interpretation is less tenable based on the dissociation kinetics at high salt concentration. An inherent point though in both hypotheses is that MC6 does not dissociate readily from the microtubule as proposed for dimeric MC1. Further support for MC6 being more tightly bound to the microtubule in the presence of ATP than MC1 is based on the equilibrium binding studies published previously (*21*). These results for monomeric MC6 indicate that the principle pathway for ATP hydrolysis is for Ncd to remain associated with the microtubule through multiple ATP turnovers.

Mt·MC6 ATPase Mechanism. In addition to the conventional methods of data fitting presented in the figures, we also analyzed the kinetics using KINSIM as described under Experimental Procedures. The mechanism and rate constants are presented in Scheme 2. The simulated traces showed good agreement with the data, and the rate constants remain essentially unchanged except for k_{+5} and k_{-5}. The MC6 kinetics of microtubule binding measured by a turbidity signal (Figure 4) were the most difficult to obtain because of the large size of the microtubule polymer relative to the MC6 monomer (M_r 42 025). The range of microtubule concentrations in which we could acquire an interpretable signal was small; therefore, k_{-5} obtained from the *y*-intercept is an estimate. Refinement of k_{-5} to 5 s^{-1} (from 3.6 ± 0.6 s^{-1}) and k_{+5} to 0.5 μM^{-1}s^{-1} (from 0.77 ± 0.11 μM^{-1} s^{-1}) provided the best fit of all the data to Scheme 2, and these constants also account for the $K_{1/2,Mt}$ at 9.6 μM.

DISCUSSION

In this study we used steady-state and pre-steady-state kinetics to define the Mt·Ncd ATPase cycle of monomeric MC6. Table 2 includes the kinetic constants derived from conventional data fitting approaches (Figures 1−9), and the mechanism is presented in Scheme 2 with the kinetic constants refined by computer simulation. This study has provided a basic understanding of Ncd as a molecular motor and has permitted direct comparison to conventional kinesin.

Our first observation was that monomeric MC6 does not show the elevated steady-state ATPase kinetics reported for monomeric kinesin (*25*, *26*, *47*, *50*, *51*). Steady-state turnover for MC6 at 1.9 s^{-1} is very similar to the k_{cat} for dimeric MC1 at 2 s^{-1} (*21*), and these results are consistent with observations published for other monomeric and dimeric Ncd constructs (*33*−*35*). Therefore, from the initial steady-state analysis, the data revealed very distinct differences in Ncd and kinesin that result upon dimerization. For kinesin, the kinetics of the dimer can be understood based on cooperative interactions between the motor domains (*14*−*16*, *23*, *47*). Yet for Ncd, the motor domains at first glance appear to be independent of each other within the dimer.

For Ncd and kinesin, there is high amino acid homology as well as structural similarity between the motor domains (*9*, *10*). However, evaluation of the kinetics for MC6 and kinesin definitely shows that there are mechanistic differences that are intrinsic to each catalytic core domain. For example, our results demonstrate that microtubule-activated ATP turnover is significantly slower for Ncd at 1.9 s^{-1} relative to dimeric kinesin (20−25 s^{-1} per site), and ADP product release limits steady-state turnover for the Mt·Ncd complex

Scheme 2: Monomeric Ncd ATPase Mechanism

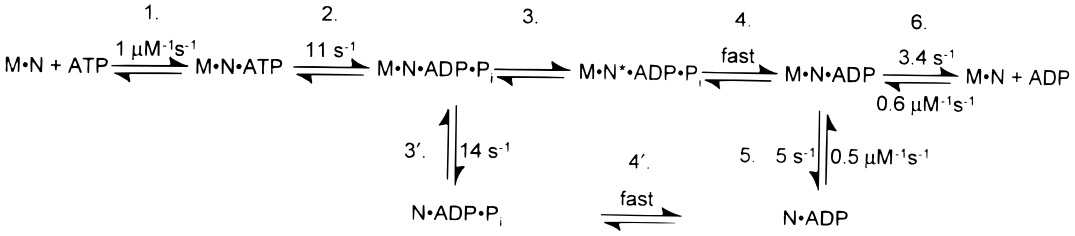

Table 2: Experimentally Determined Microtubule·MC6 Kinetic Constants

reaction	k_{+}	k_{-}	$K_{d,app}$
1. Mt·MC6 + ATP ⇆Mt·MC6·ATP	1.06 $\mu M^{-1} s^{-1}$		
2. Mt·MC6·ATP ⇆Mt·MC6·ADP·P_i	11 s^{-1}		
3. Mt·MC6·ADP·P_i ⇆Mt·MC6*·ADP·P_i	14 s^{-1}		
3′. Mt·MC6·ADP·P_i ⇆Mt + MC6·ADP·P_i	14 s^{-1}		
4′. MC6·ADP·P_i ⇆MC6·ADP + P_i	fast		
5. MC6·ADP + Mt ⇆Mt·MC6·ADP	0.77 $\mu M^{-1} s^{-1}$	3.6 s^{-1}	4.7 μM
6. Mt·MC6·ADP ⇆Mt·MC6 + ADP	3.9 s^{-1}	0.6 $\mu M^{-1} s^{-1}$	6.7 μM
k_{cat} for MC6	0.004 s^{-1}		
k_{cat} for Mt·MC6	1.9 s^{-1}		
$K_{m,ATP}$			28 μM
$K_{1/2,Mt}$			9.6 μM
$K_{d,Mt}$			0.2 μM

[Figure 5 here and Foster et al. (*20*)]. In fact, both ATP hydrolysis and the rate-limiting step are significantly slower for MC6 than for monomeric or dimeric kinesin. Therefore, these catalytic differences in kinesin and Ncd, controlled in part within the catalytic core domain, lead to the 5−10-fold slower microtubule-based motility for Ncd.

In Scheme 1, we proposed that ATP hydrolysis was required for MC6 dissociation from the microtubule. This model was based on the equilibrium binding and kinetic results which showed that the only condition that promoted MC1 or MC6 dissociation from the microtubule was ADP plus inorganic phosphate. Yet, the rate constant we determined for ATP hydrolysis (k_{+2}) was somewhat slower than the rate constant for ATP-promoted detachment from the microtubule at 14 s^{-1} (Figure 9B). Similar kinetics reported by Pechatnikova and Taylor (*33*) led them to suggest that the Ncd·ATP intermediate may dissociate from the microtubule during the ATPase cycle, a pathway more similar to skeletal muscle myosin and axonemal dynein than kinesin. To distinguish between the two pathways for ATP-promoted dissociation, we pursued experiments to compare directly monomeric MC6 with dimeric MC1 as shown in Figure 9. The amplitude data associated with the ATP-promoted dissociation kinetics support the interpretation that monomeric Ncd remains bound to the microtubule for several cycles of ATP turnover. One implication of this model is that ATP hydrolysis has become uncoupled from productive force generation because a motor domain must detach from the microtubule to reach the next microtubule binding site for movement. These results also suggest that the individual heads within the Ncd dimer are cooperative, and one function of motor domain interactions within the dimer is to weaken the microtubule binding of the adjacent head. This type of behavior has been observed for both kinesin and cytoplasmic dynein in which the monomers remain tightly bound to the microtubule at conditions that lead to motor detachment for the dimeric motor (*27*, *47*, *52*). For Ncd, we assume that the ATPase cycle regulates the transitions from the tightly bound state to a conformation more weakly bound to the microtubule. Therefore, the nucleotide state of the partner motor domain is as critical to motor detachment as the actual nucleotide state of the head poised for dissociation. Experiments are in progress to understand intermolecular interactions involving the Ncd heads and the nucleotide states that regulate these interactions.

The kinetic analysis of monomeric MC6 provided no evidence of processive ATP hydrolysis as observed for monomeric kinesins (*26*, *27*, *47*) even though the dissociation kinetics indicate that MC6 remains bound to the microtubule for several cycles of ATP hydrolysis. The experiment used to detect chemical processivity is the acid quench experiment shown in Figure 8. The data in support of chemical processivity for kinesin were a super-stoichiometric burst amplitude that correlated with the number of ATP molecules hydrolyzed per encounter with the microtubule prior to steady state. The results presented in Figure 8 as well as those reported by Pechatnikova and Taylor (*33*) do not show a burst amplitude greater than one ATP per site. However, the experimental design of the experiment presented in Figure 8 was optimized to obtain the rate constant for ATP hydrolysis rather than to investigate MC6 chemical processivity. The rapid quench experiments reported for dimeric Ncd clearly show that Ncd is not processive for ATP hydrolysis (*20*), and single-molecule motility experiments demonstrate that dimeric Ncd is not processive for motility (*18*).

The kinetic study of MC6 has led us to one part of the ATPase cycle where cooperativity between the heads of Ncd is occurring. This step is detachment from the microtubule after ATP binding. The results suggest that the second head is required either to send the signal to dissociate or to provide the mechanical impetus to force the head bound to the microtubule to release completely from the microtubule. Consideration of the results for Ncd, kinesin, and the cytoplasmic dynein with recent reports on processive monomeric kinesins such as KIF1A (*53*) opens a new avenue of research to determine an ATPase mechanism in which a single motor domain can successfully move in a processive manner along a microtubule.

ACKNOWLEDGMENT

We thank Dr. Sharyn Endow for her generous gift of the MC6 and MC1 clones used in this study, and Lori A. Bibb for preliminary studies on mantATP binding.

REFERENCES

1. Endow, S. A., Henikoff, S., and Soler-Niedziela, L. (1990) *Nature 345*, 81−83.
2. McDonald, H. B., and Goldstein, L. S. B. (1990) *Cell 61*, 991−1000.
3. Endow, S. A., and Komma, D. J. (1997) *J. Cell Biol. 137*, 1321−1336.
4. Matthies, H. J. G., McDonald, H. B., Goldstein, L. S. B., and Theurkauf, W. E. (1996) *J. Cell Biol. 134*, 455−464.
5. Kimble, M., and Church, K. (1983) *J. Cell Sci. 62*, 301−318.
6. Hatsumi, M., and Endow, S. A. (1992) *J. Cell Sci. 101*, 547−559.
7. Moore, J. D., Song, H., and Endow, S. A. (1996) *EMBO J. 15*, 3306−3314.
8. Walker, R. A., Salmon, E. D., and Endow, S. A. (1990) *Nature 347*, 780−782.
9. Kull, F. J., Sablin, E. P., Lau, R., Fletterick, R. J., and Vale, R. D. (1996) *Nature 380*, 550−555.
10. Sablin, E. P., Kull, F. J., Cooke, R., Vale, R. D., and Fletterick, R. J. (1996) *Nature 380*, 555−559.
11. Hirokawa, N. (1998) *Science 279*, 519−526.
12. Vale, R. D., and Fletterick, R. J. (1997) *Annu. Rev. Cell Dev. Biol. 13*, 745−777.
13. Stewart, R. J., Smerjian, J., and Schmidt, C. F. (1998) *Eur. Biophys. J. 27*, 353−360.
14. Gilbert, S. P., Webb, M. R., Brune, M., and Johnson, K. A. (1995) *Nature 373*, 671−676.
15. Hackney, D. D. (1995) *Nature 377*, 448−450.
16. Ma, Y., and Taylor, E. W. (1997) *J. Biol. Chem. 272*, 724−730.
17. Case, R. B., Pierce, D. W., Hom-Booher, N., Hart, C. L., and Vale, R. D. (1997) *Cell 90*, 959−966.
18. deCastro, M. J., Ho, C.-H., and Stewart, R. J. (1999) *Biochemistry 38*, 5076−5081.
19. Crevel, I. M. T. C., Lockhart, A., and Cross, R. A. (1997) *J. Mol. Biol. 273*, 160−170.
20. Foster, K. A., and Gilbert, S. P. (1999) *Biochemistry* (in press).
21. Foster, K. A., Correia, J. J., and Gilbert, S. P. (1998) *J. Biol. Chem. 273*, 35307−35318.
22. Hatsumi, M., and Endow, S. A. (1992) *J. Cell Sci. 103*, 1013−1020.
23. Gilbert, S. P., Moyer, M. L., and Johnson, K. A. (1998) *Biochemistry 37*, 792−799.
24. Hackney, D. D. (1994) *Proc. Natl. Acad. Sci. U.S.A. 91*, 6865−6869.
25. Moyer, M. L., Gilbert, S. P., and Johnson, K. A. (1996) *Biochemistry 35*, 6321−6329.
26. Ma, Y., and Taylor, E. W. (1997) *J. Biol. Chem. 272*, 717−723.
27. Jiang, W., and Hackney, D. D. (1997) *J. Biol. Chem. 272*, 5616−5621.
28. Hancock, W. O., and Howard, J. (1998) *J. Cell Biol. 140*, 1395−1405.
29. Young, E. C., Mahtani, H. K., and Gelles, J. (1998) *Biochemistry 37*, 3467−3479.
30. Kozielski, R., Sack, S., Marx, A., Thormahlen, M., Schonbrunn, E., Biou, V., Thompson, A., Mandelkow, E.-M., and Mandelkow, E. (1997) *Cell 91*, 985−994.
31. Sablin, E. P., Case, R. B., Dai, S. C., Hart, C. L., Ruby, A., Vale, R. D., and Fletterick, R. J. (1998) *Nature 395*, 813−816.
32. Chandra, R., Salmon, E. D., Erickson, H. P., Lockhart, A., and Endow, S. A. (1993) *J. Biol. Chem. 12*, 9005−9013.
33. Pechatnikova, E., and Taylor, E. W. (1997) *J. Biol. Chem. 272*, 30735−30740.
34. Lockhart, A., Cross, R. A., and McKillop, D. F. A. (1995) *FEBS Lett. 368*, 531−535.
35. Shimizu, T., Sablin, E., Vale, R. D., Fletterick, R., Pechatnikova, E., and Taylor, E. W. (1995) *Biochemistry 34*, 13259−13266.
36. Gilbert, S. P., and Johnson, K. A. (1993) *Biochemistry 32*, 4677−4684.
37. Hiratsuka, T. (1983) *Biochim. Biophys. Acta 742*, 496−508.
38. Woodward, S. K. A., Eccleston, J. F., and Geeves, M. A. (1991) *Biochemistry 30*, 422−430.
39. Barshop, B. A., Wrenn, R. F., and Frieden, C. (1983) *Anal. Biochem. 130*, 134−145.
40. Hackney, D. D. (1988) *Proc. Natl. Acad. Sci. U.S.A. 85*, 6314−6318.
41. Shimizu, T., and Morii, H. (1998) *Biochemistry 37*, 10080−10085.
42. Hirose, K., Lockhart, A., Cross, R. A., and Amos, L. A. (1996) *Proc. Natl. Acad. Sci. U.S.A. 93*, 9539−9544.
43. Sosa, H., Dias, D. P., Hoenger, A., Whittaker, M., Wilson-Kubalek, E., Sablin, E., Fletterick, R. J., Vale, R. D., and Milligan, R. A. (1997) *Cell 90*, 217−224.
44. Hoenger, A., Sack, S., Thormahlen, M., Marx, A., Muller, J., Gross, H., and Mandelkow, E. (1998) *J. Cell Biol. 141*, 419−430.
45. Crevel, I. M. T. C., Lockhart, A., and Cross, R. A. (1996) *J. Mol. Biol. 257*, 66−76.
46. Lymn, R. W., and Taylor, E. W. (1971) *Biochemistry 10*, 4617−4624.
47. Moyer, M. L., Gilbert, S. P., and Johnson, K. A. (1998) *Biochemistry 37*, 800−813.
48. Berliner, E., Young, E. C., Anderson, K., Mahtani, H. K., and Gelles, J. (1995) *Nature 373*, 718−721.
49. Chandra, R., and Endow, S. A. (1993) *Methods Cell Biol. 39*, 115−127.
50. Rosenfeld, S. S., Rener, B., Correia, J. J., Mayo, M. S., and Cheung, H. C. (1996) *J. Biol. Chem. 259*, 11908−11919.
51. Jiang, W., Stock, M. F., Li, X., and Hackney, D. D. (1997) *J. Biol. Chem. 272*, 7626−7632.
52. Iyadurai, S. J., Li, M.-G., Gilbert, S. P., and Hays, T. S. (1999) *Curr. Biol. 9*, 771−774.
53. Okada, Y., and Hirokawa, N. (1999) *Science 283*, 1152−1157.

BI991918+